1-1-1996

Partial Photoionization Cross Sections And Photoelectron Angular Distributions For Double Excitations Up To The N=5 Threshold In Helium

A. Menzel
University of Central Florida

S. P. Frigo
University of Central Florida

S. B. Whitfield
University of Central Florida

C. D. Caldwell
University of Central Florida

M. O. Krause

Partial photoionization cross sections and photoelectron angular distributions for double excitations up to the $N=5$ threshold in helium

A. Menzel,* S. P. Frigo,† S. B. Whitfield,‡ and C. D. Caldwell
Department of Physics, University of Central Florida, Orlando, Florida 32816-2385

M. O. Krause
Oak Ridge National Laboratory, Oak Ridge, Tennessee 37831-6201

(Received 12 January 1996)

Partial photoionization cross sections σ_n and photoelectron angular distributions β_n were measured for all possible final ionic states $He^+(n)$ in the region of the double excitations $N(K,T)^A$ up to the $N=5$ threshold. At a photon energy bandpass of 12 meV below the thresholds $N=3,4$, and 5, this level of differentiation offers the most critical assessment of the dynamics of the two-electron excitations to date. The experimental data are very well described by the most advanced theoretical calculations. Weaker double-excitation series with $K=N-4$ are clearly visible in the β_n data, and even previously unobserved extremely weak series members with $A=-1$ can be discerned, showing the high sensitivity of the angular resolved measurements. The shapes of the resonance-induced variations of σ_n or β_n in the double excitations below a given threshold N change radically depending on the final ionic state n but display striking similarities when comparing the satellite states with $n=N-1$ and $n=N-2$ below each threshold N. These systematic patterns may indicate a general rule for the underlying two-electron dynamics. [S1050-2947(96)02009-4]

PACS number(s): 32.80.Dz, 32.80.Fb

I. INTRODUCTION

The double excitations of helium offer an ideal case for investigating electron-electron correlations. On the one hand, the corresponding absorption spectra, first observed by Madden and Codling, [1] show very strong electron-electron correlations [2]; on the other hand, helium represents a prototype three-body system, making it a benchmark for the study of three-body dynamics. In recent years, the development of high-resolution monochromators at synchrotron radiation sources and refined calculational methods have led to substantial advances in experiment [3–5] and theory [5–22]. However, high-resolution work has remained restricted to total *absorption* measurements, [3–5] and the desirable critical comparison with theory at the level of detail of partial photoionization cross sections and photoelectron angular distribution parameters has remained elusive, despite several isolated early measurements made with the modest resolution then available [23–30]. Third-generation synchrotron radiation sources now provide the resolving power and brightness necessary to allow *electron emission* measurements which can delineate these properties at the desirable high resolution.

We have performed a study of the decay of the $^1P^o$ double excitations of helium arising from the ground state $^1S^e$ and present here the partial photoionization cross sections σ_n and photoelectron angular distributions β_n for all possible final ionic states in the region of the double excitations up to the $N=5$ threshold. This work discusses all the experimental results in detail; brief accounts of the $N=2$ and $N=5$ series have been given recently [31,32].

The resonance series are identified in the $N(K,T)_i^A$ notation of the double excitations, [6,8] where N refers to the ionization limit of the series, i is the running index of the Rydberg series, and $(K,T)^A$ represent a set of correlation quantum numbers. The hydrogenlike final state is referred to as $He^+(n)$, so that the resonant photoionization process may be described by

$$He(1s^2)+h\nu \rightarrow He^*N(K,T)_i^A \rightarrow He^+(n)+e^-.$$

In an independent particle picture N and i correspond to the principal quantum numbers of the inner and the outer electrons, respectively. Angular correlation between the two electrons is described by K and T [6], whereas the radial correlation is related to the quantum number $A=+1,-1$, or 0 [8]. In doubly excited states labeled by $A=+1$, the two electrons tend to approach or move away from the nucleus in phase, whereas in $A=-1$ states one electron approaches the nucleus while the other electron moves away from it (out-of-phase radial motion). States with $A=0$ exhibit little radial correlation since one of the electrons tends to remain far away from the nucleus while the other stays close in, showing no obvious phase relationship [9]. A more detailed description of the meaning of these quantum numbers is given elsewhere [8,15,22]. The bending vibrational quantum number $z=\frac{1}{2}(N-1-K-T)$ describes the radial correlation in the three-body system in analogy to a triatomic molecule [9]. The notation $A=+1,-1$ is replaced in the following by $A=+,-$, respectively. The $1s^2$ ground state of helium is represented by $1(0,0)^+$ in this scheme.

*Electronic address: alm@phys.physics.ucf.edu
†Present address: Physics Dept. E20, Technical University of Munich, D-85747 Garching, Germany.
‡Present address: Dept. of Chemistry, University of Nevada, Las Vegas, NV 89154-4003.

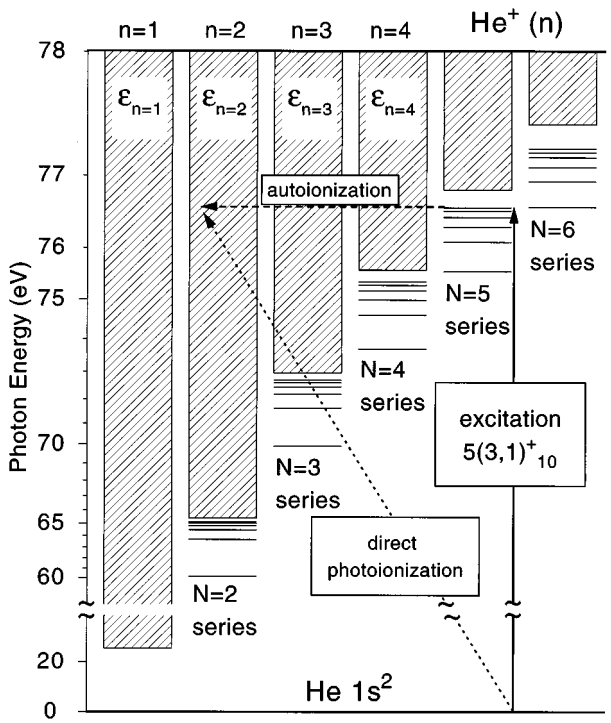

FIG. 1. Energy diagram of continua (shaded areas) and the first six discrete levels of the strongest double excitations. Double excitations, in the example displayed $5(3,1)^{+}_{10}$ (vertical arrow), followed by autoionization of this resonance (dashed horizontal arrow), and direct photoionization (dotted arrow) both contribute to the photoionization process, shown here for $He^{+}(n=2)$ only.

The weakest of all possible $2N-1$ series have been observed only in the case of $N=2$ [4]. This is due to the fact that the probability of an excitation below a threshold N rapidly decreases with increasing N. Propensity rules for photoabsorption have been proposed, $\Delta A=0$, $\Delta T=1$, and $\Delta z=0$, which can be qualitatively understood in classical terms [8,9,12]. According to these rules, the dominant series excited via dipole transitions from the $1(0,0)^{+}$ ground state should have the quantum numbers $T=1$, $A=+$, and $K=N-2$.

In the level scheme in Fig. 1 the first members of the major series are indicated by the horizontal lines converging to the various ionization thresholds $He^{+}(n)$. In the case of a double excitation, the autoionization of this excitation interferes with the direct photoionization process [33]; both pathways are shown in Fig. 1 for $n=2$. Their interference induces sharp variations of all partial cross sections and the photoelectron angular distributions, except for $n=1$, where $\beta_{n=1}=2$. A measurement of these partial quantities versus photon energy yields, therefore, a highly differentiated, although not complete, picture of the double-excitation resonances which can be checked against theory at an unprecedented level of detail.

As a consequence of the above-mentioned propensity rules, some evidence of weaker series with $N\geqslant 3$ and a higher bending vibrational number $z=1$ or $K=N-4$ has been seen only in the latest high-resolution absorption spectra [5] and, apart from excitations to $2(1,0)^{-}_{i}$ which were already observed in the experiment by Madden and Codling, [1] no evidence for the very weak series members with $A=-1$ has been found thus far. We show in this work that a measurement of the extremely sensitive angular distribution parameter reveals the weaker series with $K=N-4$ more clearly and even allows discernment of members of an $A=-1$ series.

II. EXPERIMENTAL PROCEDURES

The experiment was performed at the Advanced Light Source on the undulator beamline 9.0.1, whose design characteristics [34] and performance in emission experiments have been described before [31]. The storage ring was operated at 1.5 GeV with 400 mA at injection, and the radiation from the 8 cm, 55 period undulator was monochromatized by a spherical grating monochromator (925 lines/mm) with a movable exit slit [34]. This setup, with 10 μm entrance and 20 μm exit slits, provides a flux of approximately 10^{12} photons per second at a resolving power of up to 10 000 in a spot size of about $0.1\times 1\,\mathrm{mm}^2$ in the source region of our electron spectrometer. Our apparatus and procedures are described in detail elsewhere [35,36]. Briefly, electrons are detected simultaneously in two spherical sector plate electrostatic analyzers mounted on a rotatable platform perpendicular to the photon beam. The source volume seen by the analyzers is roughly $0.3\times 4\times 0.9\,\mathrm{mm}^3$. Since the analyzers have a small angular acceptance of 2.5(5)° half angle, no correction of the measured angular distribution was necessary. The number of electrons emitted in the direction of angle θ with respect to the major polarization axis is, in the dipole approximation, given by

$$\frac{d\sigma_n}{d\Omega}(\theta)=\frac{\sigma_n}{4\pi}\left(1+\frac{\beta_n}{4}[1+3P\cos(2\theta)]\right).$$

The degree of linear polarization P of the incoming synchrotron radiation was determined to be $P=0.97(1)$ at $h\nu=71.3$ eV by measuring the known angular distribution of neon $2s$ ($\beta=2$) and $2p$ [$\beta=1.27(5)$ [37]] photoelectrons at 36 angles. A subsequent scan of the helium $1s$ photoelectron angular distribution established a constant polarization over the undulator peak and in the entire photon energy range used. We recorded spectra at $\theta=0°$ and 90° with respect to the polarization direction and, additionally, at the pseudomagic angle $\theta_m=\frac{1}{2}\cos^{-1}(-1/3P)=55°$. At θ_m the *relative* partial cross sections σ_n(rel) were obtained directly, and the data at $\theta=0°$ and 90° yielded both the photoelectron angular distribution parameters β_n as well as σ_n(rel). The cross sections measured in both ways were virtually identical. However, the data derived from the angular distribution measurements have better statistics and are, therefore, displayed in this work. Spectra were normalized to the photon intensity and corrected for background and analyzer transmission. At a constant helium pressure of 10^{-2}Pa in the interaction region, no pressure corrections were needed. In order to check the consistency of the data and to improve statistics the spectra were generally repeated, independently normalized, compared, and averaged.

Photoelectron spectra were collected in two different modes, as shown in Fig. 2: the traditional photoelectron spectrometry (PES) mode, in which spectra are recorded at a

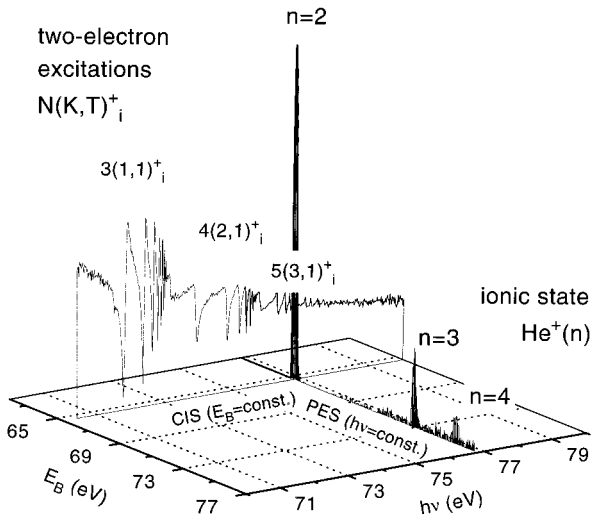

FIG. 2. Display of a normal photoelectron spectrum (PES), taken at a fixed photon energy versus binding energy, and constant-ionic-state (CIS) scan, taken at fixed binding energy versus photon energy.

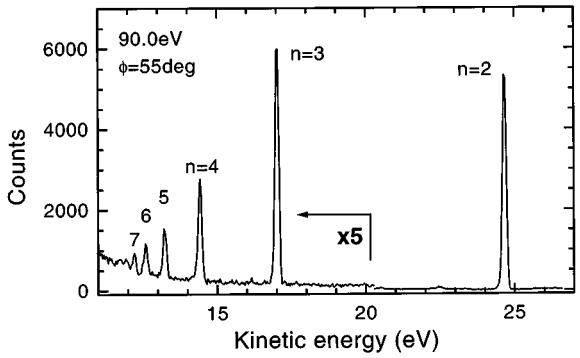

FIG. 3. PES spectrum taken at the pseudomagic angle and $h\nu = 90.0$ eV with an electron spectrometer resolution of about 70 meV. Recording time is 2000 seconds.

fixed photon energy while scanning the pass energy of the analyzers, thus yielding a spectrum of the photoelectron lines versus binding energy; and the constant-ionic-state (CIS) mode, in which spectra are recorded by simultaneously scanning the incident photon energy and the pass energy of the analyzers so as to always observe electrons which correspond to the same final ionic state, thus yielding the intensity of a given photoelectron line versus photon energy. Undulator gap and exit slit position were fixed and optimized at a photon energy near the center point of each CIS scan. According to calculations of the optical performance of the beamline, [38] a change in the monochromator resolution due to a fixed exit slit is less than 0.1 meV per eV in the photon energy ranges used and, hence, could be neglected.

The relative intensities of the photoelectron lines known from our PES measurements and the relative and absolute cross sections given by Bizau and Wuilleumier [39] were used to place the various CIS scans on an absolute scale as described below in Sec. III A. This procedure allows us to make a sensitive comparison between experiment and theory for the absolute σ_n of each partial channel that can be populated by the decay of the various resonances. Similarly, the β curves derived from the CIS scans were matched with the β data obtained in the PES mode taken directly before and after each CIS scan. The experimental errors associated with the average values of the parameters in a CIS scan are therefore given essentially by systematic errors of the PES measurements, which are primarily due to errors in the calibration of the analyzers. These errors might shift the CIS scans as *a whole*. However, the *relative* behavior of the interference structure in σ_n and β_n recorded with a CIS measurement is much more accurate and is reflected in the statistical errors seen from the scatter of the data points within a given CIS scan.

Since photoelectron spectrometry cannot resolve the nl sublevels of the hydrogenlike final ionic state, the measured partial cross sections and photoelectron angular distributions correspond to sums and weighted sums of the sublevel parameters, respectively:

$$\sigma_n = \sum_l \sigma_{nl}, \quad \beta_n = \sum_l \sigma_{nl}\beta_{nl}/\sigma_n, \quad \beta_{nl}(l=0) = 2.$$

The electron spectrometers were set to resolve the single final states $n = 1,2,3,4$ of the ion only, and, except for one high-resolution spectrum at 90.0 eV, could therefore be run at relatively low resolution, about 250 meV full width at half maximum (FWHM) in this work. The resolution of the CIS scan depends in this case solely on the bandpass of the monochromator, which was determined to be 12(3) meV for the $N = 3,4,5$ resonances by comparison with absorption data [3,5] and 6.5(2)meV by a bootstrap method for the resonances below $N = 2$ [31].

The absolute photon energy was adjusted to theoretical resonance positions [21] in the $N = 5$ series, using $2R_{\mathrm{He}} = 27.20767$ eV (R_{He} is the Rydberg constant for helium) and a double ionization potential of 79.003 44 eV. The experimental $N = 2$ to 5 resonance positions determined by the corresponding absorption measurement [3,5] are slightly higher (overall shift 8 meV).

III. RESULTS AND DISCUSSION

A. Relative partial cross sections from PES

This section compares our relative partial cross sections of the helium satellites at 90.0 eV with the results of other authors and describes the normalization procedure of our CIS scans based on measurements of the relative cross sections at 76.8 eV and 75.5 eV.

A high-resolution PES spectrum of the helium satellites as recorded with an analyzer bandpass of 70 meV at 90.0 eV at the pseudomagic angle is shown in Fig. 3. This spectrum yields, after background subtraction and transmission correction, the relative intensities of the satellites up to $n = 7$. The photon energy chosen allows a comparison, given in Table I, with results of other experiments [24,26,39–41]. We note that the spectral intensities are expected to change but little in the 90 to 100 eV photon energy interval. Our data are in very good agreement with the most recently published intensities [41]. The largest disagreement between the various ex-

TABLE I. Relative partial photoionization cross sections σ_n of helium at 90.0 eV with respect to the $n=2$ satellite.

n	This work (90.0 eV)	Ref. [39] (90.0 eV)	Ref. [40] (89.5 eV)	Refs. [24,26] (90.0 eV)	Ref. [41] (96.5 eV)
1		1265	1224	1111	1511
2	100	100	100	100	100
3	15.6(9)	19.5	18.5	14.4	15.6
4	5.7(5)		7.0	4.7	5.7
5	2.5(3)		3.5		2.7
6	1.5(2)		2.1		1.5
7	0.8(2)		1.2		0.95

periments occurs for the ratio of $n=1$ and $n=2$, which we did not measure at 90 eV.

Table II shows the relative intensities measured in the double-excitation region at 76.80 eV. Resonances in this region are very narrow and are averaged out even at our small photon bandpass of 12 meV. These intensities were averaged with the recommended values of Bizau and Wuilleumier [39] and then used for normalizing our CIS scans. The broad bandpass data points in Ref. [39] at 78.0 and 80.0 eV, which were used for extrapolation of the relative cross section in Table II, are not affected by resonances either. Therefore averaging should increase the accuracy of the partial cross sections presented. The averaged relative values were converted to absolute partial cross sections σ_n(abs) by normalization to $\sigma_{\rm tot}=780(10)$kb at this energy as the recommended value, [39] which utilizes the most accurate measurements of $\sigma_{\rm tot}$ up to 1994.

A second data set used for normalization was recorded at 75.50 eV and is given in Table III. The relative cross sections recommended in [39] were not used in this region, since the data for the satellites at 74.0 eV, measured by Bizau and Wuilleumier with a bandpass of about 400 meV, [39] are affected by the first member of the dominant $N=4$ series. In this case, different bandpasses yield different relative intensities, and averaging would lower the accuracy of the data. However, the absolute *total* cross section around 74.0 eV, $\sigma_{\rm tot}=813(10)$ kb, is not dependent on the bandpass (see, e.g., Fig. 9) and was used for the normalization of our relative cross sections.

B. High-resolution CIS scans of σ_n and β_n

1. Overview

In this section we present the high-resolution CIS measurements. Monochromator bandpass and monochromator step size were generally 12 meV and 2 meV, respectively, unless otherwise stated explicitly in the text or the figure captions. Figure 4(a) displays a wide-range scan of the $n=2$ partial cross section which gives an overview of the observed resonances below the $N=3,4$, and 5 thresholds.

The major series converging to the different thresholds are readily identified by comparison with the energy positions of the first six resonances (see also Fig. 1) below each threshold. The dashed frames in the upper panel indicate the regions of the double-excitation spectrum for which σ_n and β_n will be presented in the following subsections.

The overview of the β parameter of the $n=2$ satellite in the lower panel compares the present results with former broad bandpass experiments. The agreement is generally very good, except for a slightly higher $\beta_{n=2}$ value measured by Zubek *et al.* [29] (not shown) at higher energies. In order to minimize systematic errors, $\sigma_{n=2}$ and $\beta_{n=2}$ parameters obtained from the detailed scans with smaller step width were compared with the results of this overview scan during the two weeks of the measurements. Since no significant deviations were seen, all data presented in the following give a consistent picture of β_n.

For $N\geqslant 4$, the lowest member of series N overlaps with higher members of the series $N-1$, leading to interference effects between the series, which have been recently investigated in absorption [5]. As seen from the resonance positions in Figs. 1 and 4, the region of overlap of the first member of the major $N=6$ series with the members $i=9,10,11,12$ of the $N=5$ series offers the best possibility to investigate this interseries interference. This part of our measurements places the most exacting demands on both experiment and theory and has been published separately [32].

2. N=2 resonances

The series terminating on the $N=2$ threshold are well known from absorption measurements [1,3,4] and we re-

TABLE II. Relative and absolute partial photoionization cross sections σ_n of helium at 76.8 eV used for normalization of the CIS scans with respect to the $n=1$ main line.

	σ(rel) (in % of $n=1$)			
n	This work	Ref. [39]	Average	σ(abs) (kb) [a]
1	100	100	100	694(14)
2	9.5(7)	9.1	9.3(5)	65(3)
3	2.3(3)	1.7	2.0(2)	13.9(14)
4	1.04(10)	1.01	1.03(10)	7.1(7)

[a]Normalized to $\sigma_{\rm total}=780$ kb [39].

TABLE III. Relative and absolute partial photoionization cross sections σ_n of helium at 75.5 eV used for normalization of the CIS scans with respect to the $n=1$ main line.

	σ(rel)(in % of $n=1$)	
n	This work	σ(abs) (kb) [a]
1	100	723(15)
2	10.3(9)	75(7)
3	2.05(30)	15(2)

[a]Normalized to $\sigma_{\rm total}=813$ kb [39].

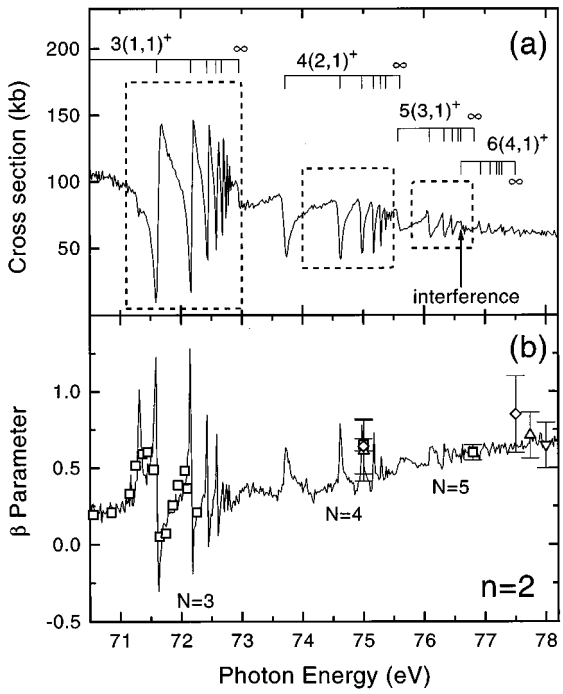

FIG. 4. (a) Partial cross section of the $n=2$ final ionic state as determined from two wide-range high-resolution (approximately 12 meV) CIS scans, taken with a step width of 20 meV at $\theta=0°$ and $\theta=90°$. (b) $\beta_{n=2}$ parameter (solid line) derived from the same scans. PES measurements of various authors are indicated by the open symbols: (□) Lindle *et al.*, Ref. [24]; (◇) Bizau *et al.*, Ref. [42]; (△) Schmidt *et al.*, Ref. [43]; (▽) Wehlitz *et al.*, Ref. [44].

ported recently the results of an electron emission measurement [31]. To complement our results for the higher series, we present in Fig. 5 the resonances of the $N=2$ series as observed in a CIS scan at a bandpass of 6.5 meV. Comparison of this scan, taken at $\theta=0°$, with a scan taken at $\theta=90°$ yielded $\beta_{n=1}=2$ as required. Both the dominant $2(0,1)_i^+$ and the weak $2(1,0)_i^-$ series can be seen, and a very good accord with the ion-yield spectrum [3] is noted. However, no attempt was made to resolve the very weak and sharp $2(-1,1)_i^+$ series observed recently [4]. The effect of finite resolution of the monochromator is best seen by the nonvanishing signal at the cross section minima. According to Fano, [33] in the case of only one available continuum channel [here $He^+(1s)+\epsilon p$] the cross section measured with infinite resolution should drop to zero in these separated resonances, indicating complete correlation of resonance and continuum. As described elsewhere, [31] the analysis of the

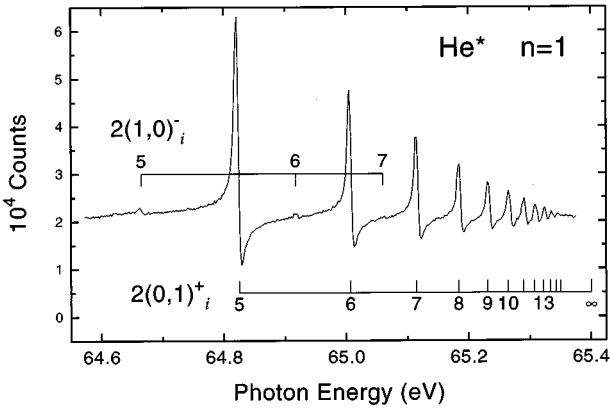

FIG. 5. CIS scan of the $He^+(n=1)$ main line below the $N=2$ threshold (see also Ref. [31]). Note the appearance of the weak $2(1,0)^-$ series.

$i=5$ to 7 members of the dominant series yields widths Γ_i and Fano shape parameters q_i [33] that are in good agreement with recent theoretical results, [10,17] but slightly lower than the latest experimental results (see Table IV). From our data we derive a reduced width of $\Gamma_i(i^*)^3=200(20)$, where i^* is the effective quantum number.

3. N=3 resonances

In the region below the $N=3$ threshold the continuum channels of the main line, $n=1$, and the first satellite, $n=2$, are open. The corresponding partial cross sections, derived from the scans taken at $\theta=0°$ and $\theta=90°$, are displayed in the lower two panels of Fig. 6. In order to show how the profiles of the partial cross sections add up, the total cross section is also included in the upper panel of this figure. The dominant Rydberg series $3(1,1)^+$ is seen in both partial and the total cross sections up to the members $i=9$ or 10. Whereas the resonances appear in very different shapes in the continuum channels, the resonance-induced *variations* in both channels, which are for the member $i=4$ about 88 kb in the $n=1$ and 136 kb in the $n=2$ channel, are of the same order of magnitude. However, the correlation between the resonances and the continua is much stronger for the $n=2$ channel, because the *relative* variations are much larger. The minimum value of the $n=2$ partial cross section is only 8(1)kb, showing that only about 9(2)% of the $n=2$ continuum is uncorrelated to the resonances.

The experimental data can be compared with two advanced calculations, one using the hyperspherical close-

TABLE IV. Width (in meV) and Fano q parameters of the $2(0,1)_i^+$ resonances $i=5,6,7$ determined using a bandpass of 6.5(2) meV.

	This work		Refs. [3,4]	Refs. [10,17]	
i	Γ (expt.)	q (expt.)	Γ (expt.)	Γ (theory)	q (theory)
5	1.8(3)	−2.4(2)	2.5	1.9 [a]	−2.45
6	0.9(2)	−2.6(2)	1.5	1.1 [b]	−2.41
7	0.6(2)	−2.6(2)	0.9	0.7 [b]	−2.39

[a]Reference [17].
[b]Reference [10].

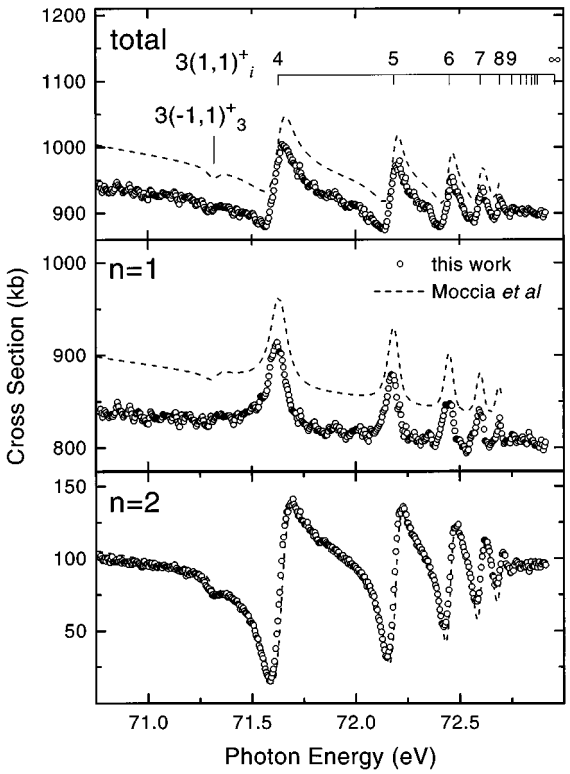

FIG. 6. Experimental and convoluted theoretical total and partial absolute cross sections below the $N=3$ threshold measured with a photon bandpass of 35 meV. Experiment: open circles; theory: dashed line, Ref. [11]. The calculation of Ref. [45] coincides with the one shown.

coupling method [45] (not shown) and the other a K-matrix L^2 basis-set calculation [11]. Both theories give almost identical results that are nearly independent of the gauge representations of the dipole operator. The theoretical data were convoluted with the experimental bandpass, which was 35 meV in this instance. Positions, widths, and shapes of the resonance-induced variations are very well described by both theories. Even the absolute values of the cross sections are in very good agreement for $n=2$ and in reasonably good agreement for $n=1$. The difference between theory and experiment for $n=1$ is about 5%, which exceeds the experimental errors of 2% [39], and the theoretical errors of 1% [32,45]. With an estimated experimental uncertainty of 5% for $\sigma_{n=2}$, the excellent agreement with the theory is somewhat accidental. The first member $i=3$ of the weaker series $3(1,-1)^+_i$ is only seen as a shallow dip in the $n=2$ partial cross section, whereas the main line $n=1$ and total cross section are hardly affected.

In sharp contrast, the angular distribution derived from the same scans of the $n=2$ satellite shows this weak member very clearly (Fig. 7), indicating that differentiation beyond the level of the partial cross section is very useful for extracting information about the weaker series. Earlier experimental data [24,29] are included in the figure in order to show their agreement with our data and the effect of monochromator resolution, changing from 170 meV [24] to 60 meV [29] and to 35 meV in our work. The accuracy of this β parameter scan is given by the systematic error of ± 0.1, which would shift the scan as a whole, and by the small statistical error,

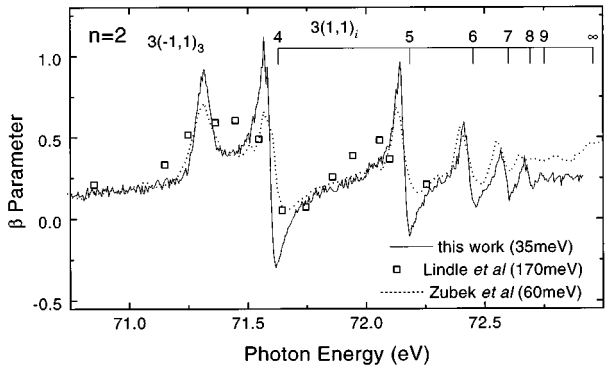

FIG. 7. Experimental β parameter of the $n=2$ satellite below the $N=3$ threshold. Data with different resolutions by different authors are included for comparison. Solid line: this work; squares: Ref. [24]; dotted line: Ref. [29].

obtainable from the scattering of the data points within the scan.

A comparison of the experimental and theoretical β parameters from our high-resolution scans (12 meV), shown in Fig. 8, reveals excellent agreement with both of the abovementioned calculations. As was the case for the partial cross sections, both theories [11,45] are identical and only the data of Moccia and Spizzo [11] are displayed. In order to compare the infinitely resolved theoretical data with the experiment, the β parameter was derived from the theoretical differential cross sections convoluted with 12 meV.

Although the relatively big step size of 20 meV within the scan may have obliterated the very sharp $3(2,0)^-$ or $3(0,0)^-$ resonances, [11] the $3(1,1)^+$ series and the $3(-1,1)^+_3$ member are now accentuated, with $3(1,1)^+_4$ nearly reaching the allowed limits of β. Other members of the weaker series $3(-1,1)^+$ are not evident in the data, since their energy positions are very close to the main series $3(1,1)^+$, leading to an interference between both series [19]. The small deviation of the theoretical and experimental data in the minima of the β parameter may be caused by very small differences between the experimental and theoretical positions of the interfering series.

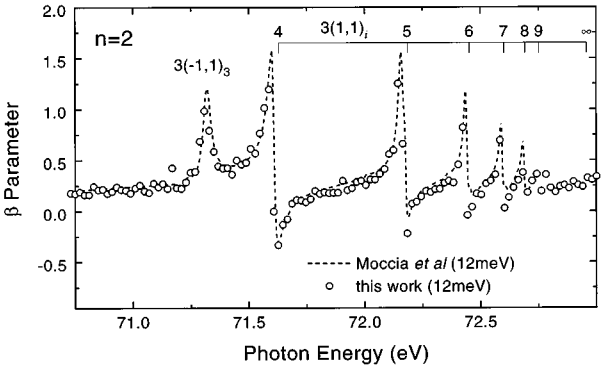

FIG. 8. Comparison of the experimental β parameter of the $n=2$ satellite below the $N=3$ threshold at 12 meV resolution (open circles) and 20 meV step width with calculations (dashed line, Ref. [11]). Another calculation (Ref. [45], not shown) gives the same result.

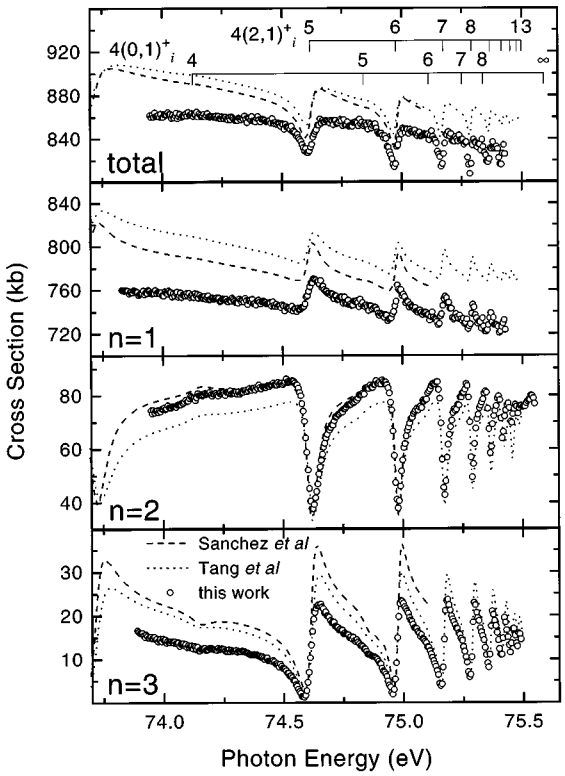

FIG. 9. Experimental and convoluted theoretical total and partial absolute cross sections below the $N=4$ threshold. Experiment: open circles; theory: dotted line, Ref. [45]; dashed line, Ref. [18].

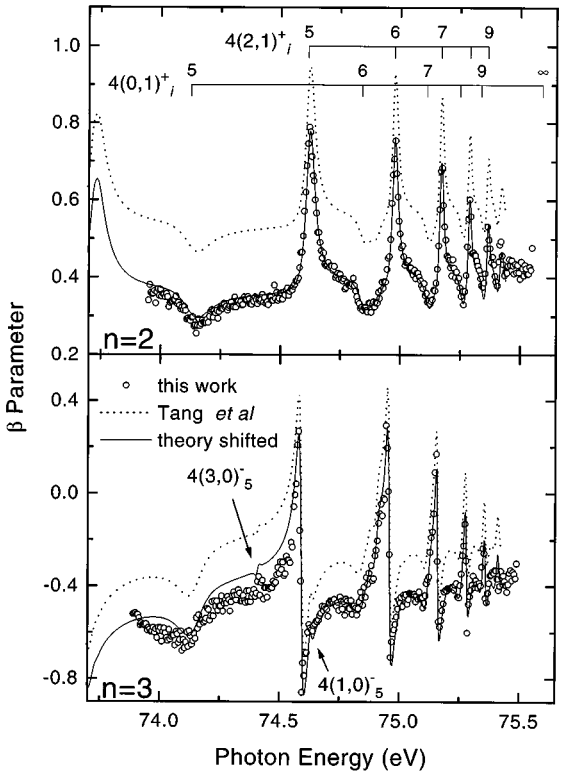

FIG. 10. Comparison of the experimental β parameters of the $n=2$ and the $n=3$ satellites below the $N=4$ threshold with convoluted theoretical results. Experiment: open circles; theory: dotted line, Ref. [45]. The solid line represents the theoretical curve shifted by -0.17 units.

4. N=4 resonances

Below the $N=4$ threshold, three different continuum channels are resolvable. As seen from Fig. 9, the general observations made in the preceding subsection also hold true for $N=4$. The major series $4(2,1)^+$ is interfering with all available continuum channels, leading to absolute variations which are roughly the same order of magnitude, 17 kb to 50 kb. However, the shape of the variations is vastly different. Again, the correlation of the continuum of the highest excited final ionic state $n=3$ with the discrete resonances of the major series is the strongest. The minima of the wider resonances, which are unaffected by the small bandpass, are about 5(2)% of the whole $n=3$ continuum cross section.

The theoretical data from two sources [18,45] agree very well regarding positions, widths, and shapes of the resonances. The error in the calculation of Tang and Shimamura is estimated to be 1%, [45] whereas the error in the data of Sánchez and Martín [18] is larger, since their velocity (not shown) and length results differ by about 5%. The theoretical and experimental absolute values of the partial cross section for $n=1$ and $n=2$ agree also within 5%, slightly exceeding the combined errors of the experimental and the theoretical data. The accuracy of the experimental data is 2% for $\sigma_{n=1}$, 10% for $\sigma_{n=2}$, and 13% for $\sigma_{n=3}$ (see Table III). The resonance-induced excursions for the first two members of the $n=3$ ionic state are noticeably smaller in the experiment than in the theory. This discrepancy exceeds the combined uncertainties of experiment and theory. The weak series $4(0,1)^+$ is not evident in the partial cross sections; only the first member $i=4$, a wide feature with little amplitude, may be discerned in the $n=3$ and $n=2$ partial cross sections.

The weak series can be readily identified in the angular distributions of both satellites (see Fig. 10). The $\beta_{n=3}$ parameter clearly exhibits the small dips associated with these resonances up to member $i=8$. Closer inspection of the experimental data even allows an assignment of members $4(3,0)_5^-$ and $4(1,0)_5^-$ [18] belonging to the very weak ''minus'' series. These resonances are quasiforbidden to autoionize according to the propensity rules mentioned earlier, but the very good statistics of the experimental data for the $n=3$ satellite allow a comparison of experimental and theoretical data for this weak member $4(1,0)_5^-$. As can be seen from Fig. 11, the experimental data in the vicinity of this weak resonance are very well described by the theory of Ref. [45].

An overall offset of theory and experiment of 0.17 units in both satellites exceeds the systematic experimental errors (± 0.1) only by 0.07 units. A uniform shift of one of the data sets (here we chose the theoretical curves) reveals a remarkable agreement in all other regards. All calculated features of the dominant $4(2,1)^+$ and the minor $4(0,1)^+$ series follow the experiment closely.

5. N=5 resonances

The most interesting feature of the region below the $N=5$ threshold is the interference occurring between the lowest member $6(4,1)_6^+$ of the major series converging to $N=6$ and higher members of the $5(3,1)^+$ series below $N=5$. A strong interference was predicted theoretically [12]

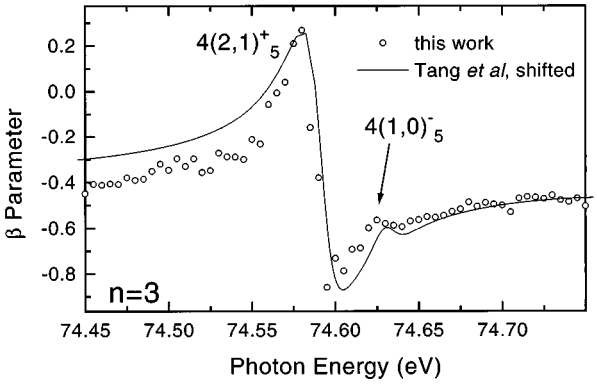

FIG. 11. Detail of the experimental and theoretical $\beta_{n=3}$ parameter from Fig. 10 in the vicinity of a very weak ''minus'' resonance. Experiment: open circles; theory: solid line (Ref. [45], shifted by -0.17 units).

because of the high correlation between series having similar characteristics (e.g., z,A) and was later observed in absorption [3,5]. The results of emission measurements over the interference region have been discussed in detail earlier [32]. For the sake of completeness we show here the most important results of that analysis.

Figure 12 shows the experimental partial cross sections and the total cross section along with the theoretical curves. The corresponding angular distributions are given in Fig. 13.

The accord between the experiment and the calculation is very good for the resonance-induced variations and is reasonable for the absolute values of σ_n. The excellent agreement in the case of $n=3$ and $n=4$ on an absolute scale is somewhat accidental. The experimental errors in the partial cross sections are evaluated to be 1.5% (total) according to, [39] and 2% ($n=1$), 5% ($n=2$), and 10% ($n=3,4$) according to the partitioning described in Sec. III A. The theoretical cross sections are accurate within 1% [32]. We attribute some small variances noted in the *relative* behavior of $\sigma_{n=1}$ to statistical scattering of the experimental data, introduced by the small relative variation of the partial cross section of about 1.5%. These variances are transferred to the sum, σ_{tot}, of all partial cross sections, which vary greatly in their resonance shapes [32].

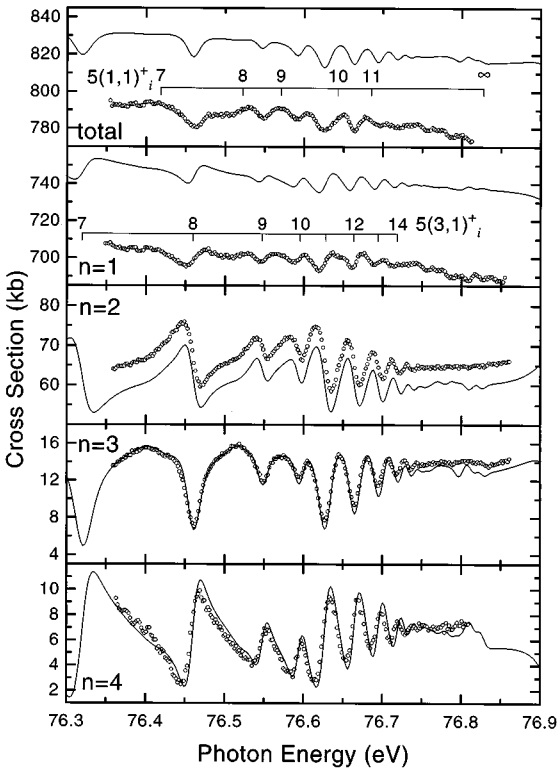

FIG. 12. Experimental and convoluted theoretical total and partial absolute cross sections in the region of the $N=5$ resonances. Experiment: open circles; theory: solid lines, Ref. [32]. The experimental data for $n=1$ and the total cross section are smoothed.

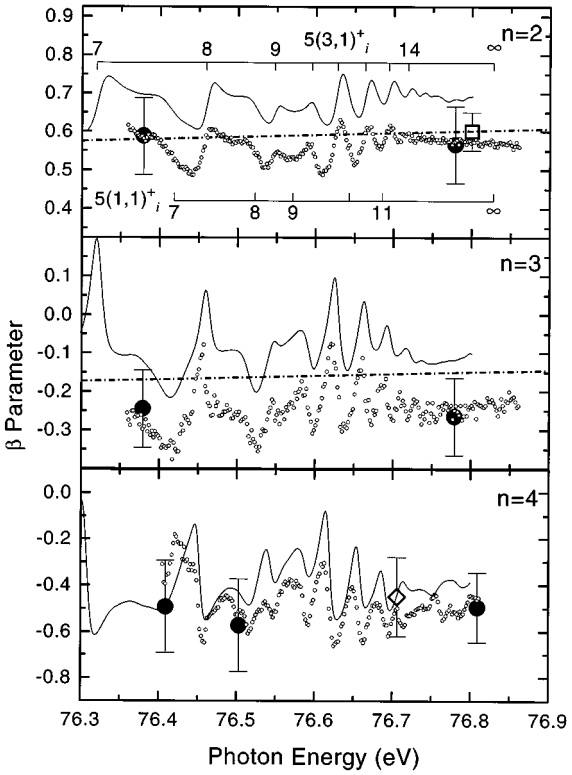

FIG. 13. Experimental and convoluted theoretical β parameters in the region of the $N=5$ resonances. Experiment: open circles; theory: solid lines, Ref. [32]. Experimental data for $n=4$ are smoothed. Solid circles (this experiment), square (Ref. [24]), and diamond (Ref. [46]) represent β values derived from PES measurements. Error bars on the solid circles indicate the systematic errors (± 0.1) of this experiment. The dot-dashed lines are interpolated from data given in Ref. [44].

As was the case with the $N=3$ and $N=4$ resonances, the absolute variation of the σ_n induced by the resonance states is of a similar magnitude for all channels n, here 11 to 22 kb, while the relative variation is smallest for $n=1$ and largest for $n=4$. Again, the correlation of the different continua with the resonances is increasing with increasing n.

In analogy to the $N=3$ and $N=4$ resonances, the weaker series is more clearly seen in the β_n parameters displayed in Fig. 13, although the members $i \geqslant 9$ are perturbed by the interference. The systematic error for the β scans is given by the accuracy of the data derived from the corresponding photoelectron spectra (± 0.1), indicated in Fig. 13 by the error bars. As is the case for σ_n, the accord between the theoretical and experimental results is also good for the β_n. This

TABLE V. Absolute peak-to-valley variation of the partial cross sections σ_n below the thresholds $N=3,4,5$.

	Variation of σ_n in kb			
N	$n=1$	$n=2$	$n=3$	$n=4$
3	88(2)	136(5)		
4	30(1)	50(2)	17(1)	
5	11(1)	22(1)	12(1)	11(1)

holds true for the amplitudes of the variations, the peak positions, and the resonance patterns. Differences are generally within the experimental uncertainties, except for the absolute magnitudes of the β_n, which slightly exceed these uncertainties for $n=2$ and $n=3$.

C. General patterns in σ_n and β_n

The overall behavior of the β_n parameters corroborates previous observations [44,46] and predictions [7] that β_n should decrease with increasing n and approach -1 for high n and low kinetic energies due to the dynamically unfavored transitions [7]. Another general trend is the similar magnitude of the peak-to-valley variation in the σ_n induced by the resonance states below a given threshold N. Table V shows these variations below the different thresholds, corrected for the finite bandpass of the experiment. If the variations are related to the ''average'' cross sections σ_n, the relative variations of the cross sections are seen to increase with increasing n below a given threshold N, reflecting the smaller continuum contribution at higher n.

The most striking similarity among the various decay paths emerges when all of the satellite partial cross sections below the different thresholds N are displayed together. As shown in Fig. 14, we find virtually the same line profiles for the decays with $\Delta N=1$ and $\Delta N=2$, where $\Delta N=N-n$, both experimentally and theoretically [45]. In the figure, the diagonal lines connect decay paths corresponding to $\Delta N=1$ (top), $\Delta N=2$ (middle), and $\Delta N=3$ (bottom). For higher N, patterns are obscured by the influence of interferences between series, [5] here seen only for the higher members of $N=5$.

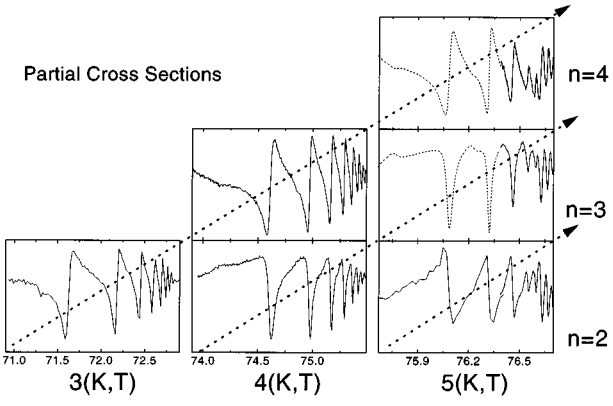

FIG. 14. Overview of the experimental partial cross sections (solid lines) of the $n=2,3,4$ satellites of helium in the region of the $N=3,4,5$ double-excitation resonances. Individual panels have different y scales. Convoluted theoretical results (dashed lines, Ref. [32]) are used in two panels for extension of the curves towards lower photon energy not covered by the experiment. The diagonal arrows indicate a possible general pattern of the decay of the resonances (see text), corresponding from top to bottom to autoionization pathways with $\Delta N=1$, $\Delta N=2$, and $\Delta N=3$, respectively.

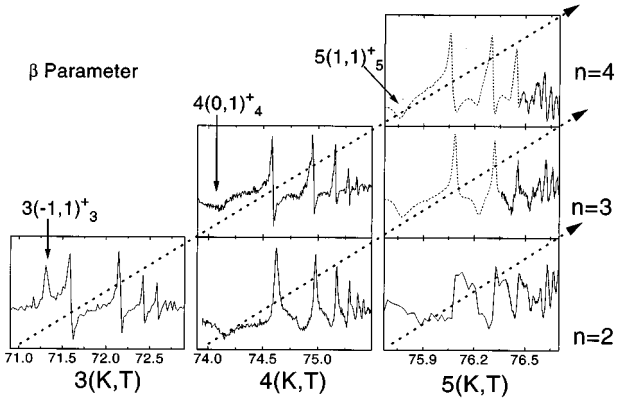

FIG. 15. Overview of the experimental β parameters (solid lines) of the $n=2,3,4$ satellites of helium in the region of the $N=3,4,5$ double-excitation resonances. Individual panels have different y scales. Convoluted and shifted theoretical results (dashed lines, Ref. [32]) are used in two panels for extension of the curves towards lower photon energy not covered by the experiment. The dotted arrows indicate the same general pattern as in Fig. 14 (see text).

The β parameters, shown in Fig. 15, exhibit the same similarities along the indicated arrows, and show additionally similarities for the weaker series with $K=N-4$, except for the $3(-1,1)_3^+$ resonance.

This overall pattern may be explained by the propensity rules for autoionization [8,12] and the general similarity of states with the same set of approximately good quantum numbers $(K,T)^A$. According to the propensity rules, [8,12] the principal decay should proceed mainly through the channel $\Delta N=1$, $\Delta K=1$, $\Delta T=0$, and $\Delta A=0$. The corresponding states have the same characteristics, i.e., their wave functions are concentrated in the same subspace in a hyperspherical description [8,12], leading to a large overlap and therefore to relatively large autoionization matrix elements. The fact that the similar profiles emerge for all decays with $\Delta N=1$, independent of the value of N, suggests that the relationship between the potential curves in the hyperspherical description mainly contributing to the $\Delta N=1$ decay is also independent of N. Under this assumption, the similarities between potential curves contributing to the decays with $\Delta N=2,3,\ldots$ follow as a matter of course.

The $n=1$ main line does not match the observed pattern. According to the interaction rules mentioned above, the smaller width of the dominant resonances $2(0,1)^+$ compared to the resonances with higher N was explained by the lack of the corresponding $1(-1,1)^+$ in $N=1$ [12]. Similarly, we deduce that the $n=1$ continuum does not match the above pattern observed within the satellites because its interaction with the resonances is very different, i.e., the doubly excited states cannot decay into the $n=1$ continuum without changing the approximately good quantum numbers.

The weaker series $N(N-4,1)^+$ decays according to the autoionization rules outlined above mainly through the con-

figuration $N-1(N-5,1)^+$, which is not allowed for $N=1,2$. Accordingly, the $n=1$ main line and the $n=2$ satellite should not fit in the decay pattern of this weaker series exhibited in our data for the $n=3,4$ satellites. The difference in the appearance of the first member in the β parameter, which is a symmetric peak in $n=2$ for $3(-1,1)_3^+$, but a symmetric dip in $n=3,4$ for the corresponding $4(0,1)_4^+$ and $5(1,1)_5^+$ resonances, corroborates the above assumptions. A difference could also be caused by the above-mentioned (see Sec. III B 3) interference with the main series $3(1,1)^+$ [19], but the relatively wide energy separation of the first member $3(-1,1)_3^+$ from the main series is likely to guarantee an unperturbed member. Extension of these systematics for weaker series or higher n could readily be done, but taking into account the weakness of further series and the small number of unperturbed series members for higher N [5], a proof of the expected systematics by experiment seems to be unlikely.

In contrast to the above argumentation, the $4(0,1)^+$ series in the $n=2$ continuum does match the pattern, i.e., it induces small dips in the β curve. Furthermore, the patterns for the weak series $K=N-4$ are the same for decays with $\Delta N=1$ and $\Delta N=2$, in contrast to the behavior of the main resonances with $K=N-2$. This cannot be readily explained in the manner outlined above. Generally, the decay patterns show nicely the similarity of states with conservation of good quantum numbers, although further theoretical investigations are needed to give a detailed explanation of this phenomenon.

IV. CONCLUSIONS

In conclusion, we measured the partial photoionization cross sections and angular distributions of all accessible final ionic states in helium in the photon energy regime of the double excitations converging to the $N=2,3,4$, and 5 thresholds. The principal series are clearly delineated in both σ_n and β_n. Due to the enhanced sensitivity of angular resolved measurements, the β_n show all minor series with $K=N-4$ very clearly, in contrast to measurements of the total absorption cross section. Furthermore, we were also able to discern very weak members with $A=-1$ in the data of the angular distribution. Very good agreement between this work and the most advanced theories was found. Notably, this agreement extends to the *absolute* partial and total cross sections. This holds true especially for the results of the hyperspherical close-coupling method, which is capable of readily handling even the higher N series.

A comparison of the σ_n of the different ionic states below the different thresholds reveals systematic patterns. These patterns are similarly exhibited in the β_n, for both the dominant $K=N-2$ series and the weaker double excitations with $K=N-4$. We tentatively propose an extension of the systematics by use of the correlation rules for the $N(K,T)^A$ states given in the literature [8,12], although further theoretical and experimental work toward understanding these features of the doubly excited states will be needed.

ACKNOWLEDGMENTS

We take pleasure in acknowledging Phil Heimann and John Bozek for their help with the beamline. We would like to thank I. Shimamura and J.-Z. Tang for providing us with the results of their calculations prior to publication. We are also grateful to R. Moccia and P. Spizzo and to I. Sánchez and R. Martín for sending us the numerical output of their published results. This work is supported by the National Science Foundation under Grant Nos. PHY-9207634 and PHY-9507573. The loan of equipment for this project by the Oak Ridge National Laboratory is gratefully acknowledged. Operation of the ALS at the LBNL is supported by the U.S. DOE under Contract No. DE-AC03-76F00098.

[1] R.P. Madden and K. Codling, Phys. Rev. Lett. **10**, 516 (1963); Astrophys. J. **141**, 364 (1965).
[2] J.W. Cooper, U. Fano, and F. Pratts, Phys. Rev. Lett. **10**, 518 (1963).
[3] M. Domke, C. Xue, A. Puschmann, T. Mandal, E. Hudson, D.A. Shirley, G. Kaindl, C.H. Greene, H.R. Sadeghpour, and H. Petersen, Phys. Rev. Lett. **66**, 1306 (1991).
[4] M. Domke, G. Remmers, and G. Kaindl, Phys. Rev. Lett. **69**, 1171 (1992).
[5] M. Domke, K. Schulz, G. Remmers, A. Gutierrez, G. Kaindl, and D. Wintgen, Phys. Rev. A **51**, R4309 (1995).
[6] D.R. Herrick and O. Sinanoglu, Phys. Rev. A **11**, 97 (1975); M.E. Kellman and D.R. Herrick, *ibid.* **22**, 1536 (1980).
[7] C.H. Greene, Phys. Rev. Lett. **44**, 869 (1980).
[8] C.D. Lin, Phys. Rev. A **29**, 1019 (1984); Adv. At. Mol. Phys. **22**, 77 (1986).
[9] S. Watanabe and C.D. Lin, Phys. Rev. A **34**, 823 (1986).
[10] P. Hamacher and J. Hinze, J. Phys. B **22**, 3397 (1989).
[11] R. Moccia and P. Spizzo, Phys. Rev. A **43**, 2199 (1991).
[12] H.R. Sadeghpour, Phys. Rev. A **43**, 5821 (1991).
[13] Y.K. Ho, Phys. Rev. A **44**, 4154 (1991).
[14] J.-Z. Tang, S. Watanabe, and M. Matsuzawa, Phys. Rev. A **46**, 2437 (1992).
[15] A.R.P. Rau, Science **258**, 1444 (1992).
[16] J.-Z. Tang, S. Watanabe, M. Matsuzawa, and C.D. Lin, Phys. Rev. Lett. **69**, 1633 (1992).
[17] T.C. Chang, Phys. Rev. A **47**, 3441 (1993).
[18] I. Sánchez and F. Martín, Phys. Rev. A **48**, 1243 (1993).
[19] D. Wintgen and D. Delande, J. Phys. B **26**, L399 (1993).
[20] A.G. Abrashkevich and M. Shapiro, Phys. Rev. A **50**, 1205 (1994).
[21] J.-Z. Tang and I. Shimamura, Phys. Rev. A **50**, 1321 (1994).
[22] C.D. Lin, Phys. Rep. **257**, 1 (1995).
[23] P.R. Woodruff and J.A.R. Samson, Phys. Rev. A **25**, 848 (1982).
[24] D.W. Lindle, T.A. Ferrett, U. Becker, P.H. Kobrin, C.M. Truesdale, H.G. Kerkhoff, and D.A. Shirley, Phys. Rev. A **31**, 714 (1985).
[25] J. Jiménez-Mier, C.D. Caldwell, and D.L. Ederer, Phys. Rev. Lett. **57**, 2260 (1986).

[26] D.W. Lindle, P.A. Heimann, T.A. Ferrett, and D.A. Shirley, Phys. Rev. A **35**, 1128 (1987).
[27] H. Kossmann, B. Krässig, and V. Schmidt, J. Phys. B **21**, 1489 (1988).
[28] M. Zubek, G.C. King, P.M. Rutter, and F.H. Read, J. Phys. B **24**, L337 (1991).
[29] M. Zubek, G. Dawber, R.I. Hall, L. Avaldi, K. Ellis, and G.C. King, J. Phys. B **24**, L337 (1991).
[30] M.O. Krause, S.B. Whitfield, C.D. Caldwell, J.-Z. Wu, P. van der Meulen, C.A. de Lange, and R.W.C. Hansen, J. Electron. Spectrosc. Relat. Phenom. **58**, 79 (1992).
[31] C.D. Caldwell, A. Menzel, S.P. Frigo, S.B. Whitfield, and M.O. Krause, Sync. Rad. News **8**, 23 (1995).
[32] A. Menzel, S.P. Frigo, S.B. Whitfield, C.D. Caldwell, M.O. Krause, J-Z. Tang, and I. Shimamura, Phys. Rev. Lett. **75**, 1479 (1995).
[33] U. Fano, Phys. Rev. **124**, 1866 (1961).
[34] P. Heimann, T. Warwick, M. Howells, W. McKinney, D. Digennaro, B. Gee, D. Yee, and B. Kincaid, Nucl. Instrum. Methods A **319**, 106 (1992).
[35] M.O. Krause, T.A. Carlson, and A. Fahlman, Phys. Rev. A **30**, 1316 (1984).
[36] S.B. Whitfield, M.O. Krause, P. van der Meulen, and C.D. Caldwell, Phys. Rev. A **50**, 1269 (1994).
[37] F.J. Wuilleumier and M.O. Krause, J. Electron. Spectrosc. Relat. Phenom. **15**, 15 (1976).
[38] P.A. Heimann (private communication).
[39] J.M. Bizau and F. Wuilleumier, J. Electron. Spectrosc. Relat. Phenom. **71**, 205 (1995).
[40] U. Becker and D.A. Shirley, in *VUV- and Soft X-ray Photoionization*, edited by U. Becker and D.A. Shirley (Plenum Press, New York, 1996).
[41] S. Svensson, A. Kikas, A. Ausmees, S.J. Osborne, S. Aksela, A. Naves de Brito, and E. Nommiste, J. Phys. B **28**, L293 (1995).
[42] J.M. Bizau, F. Wuilleumier, P. Dhez, D.L. Ederer, T.N. Chang, S. Krummacher, and V. Schmidt, Phys. Rev. Lett. **48**, 588 (1982).
[43] V. Schmidt, H. Derenbach, and R. Malutzki, J. Phys. B **15**, L523 (1982).
[44] R. Wehlitz, B. Langer, N. Berrah, S.B. Whitfield, J. Viefhaus, and U. Becker, J. Phys. B **26**, L783 (1993).
[45] J.-Z. Tang and I. Shimamura (unpublished).
[46] P.A. Heimann, U. Becker, H.G. Kerkhoff, B. Langer, D. Szostak, R. Wehlitz, D.W. Lindle, T.A. Ferrett, and D.A. Shirley, Phys. Rev. A **34**, 3782 (1986).